Human Molecular Genetics, 2021, Vol. 30, No. 11 985–995

doi: 10.1093/hmg/ddab077
Advance Access Publication Date: 31 March 2021
General Article

GENERAL ARTICLE

Generation and characterization of a *P2rx2* V60L mouse model for DFNA41

Xiaoya Chen[1,2], Clemer Abad[3], Zheng-yi Chen[4], Juan I. Young[3,6], Channabasavaiah B. Gurumurthy[5], Katherina Walz[3,6,†*] and Xue Zhong Liu[1,6,*]

[1]Department of Otolaryngology, University of Miami Miller School of Medicine, Miami, FL 33136, USA, [2]Department of Otolaryngology, Xiangya Hospital, Central South University, Changsha, Hunan 410008, China, [3]John P. Hussman Institute for Human Genomics, University of Miami Miller School of Medicine, Miami, FL 33136, USA, [4]Department of Otolaryngology and Program in Neuroscience, Harvard Medical School and Eaton Peabody Laboratory, Massachusetts Eye and Ear Infirmary, Boston, Massachusetts 02114, USA, [5]Mouse Genome Engineering Core Facility, Vice Chancellor for Research Office, University of Nebraska Medical Center, Omaha, NE 68198, USA and [6]Dr. John T. Macdonald Foundation Department of Human Genetics, University of Miami Miller School of Medicine, Miami, FL 33136, USA

*To whom correspondence should be addressed at: University of Miami Miller School of Medicine, 1120 NW 14th Street, 5th Floor, Miami, FL 33136, USA. Tel: (305)243-1451; Fax: (305)243-2009; Email: xliu@med.miami.edu

Abstract

P2RX2 encodes the P2X2 receptor, which is an adenosine triphosphate (ATP) gated (purinoreceptor) ion channel. P2RX2 c. 178G > T (p.V60L) mutation was previously identified in two unrelated Chinese families, as the cause of human DFNA41, a form of dominant, early-onset and progressive sensorineural hearing loss. We generated and characterized a knock-in mouse model based on human p.V60L mutation that recapitulates the human phenotype. Heterozygous KI mice started to exhibit hearing loss at 21-day-old and progressed to deafness by 6-month-old. Vestibular dysfunction was also observed in mutant mice. Abnormal morphology of the inner hair cells and ribbon synapses was progressively observed in KI animals suggesting that *P2rx2* plays a role in the membrane spatial location of the ribbon synapses. These results suggest that P2rx2 is essential for acoustic information transfer, which can be the molecular mechanism related to hearing loss.

Introduction

Disabling hearing loss (HL) directly affects 466 million people worldwide (https://www.who.int/news-room/fact-sheets/detail/deafness-and-hearing-loss). The high prevalence/incidence of hearing loss in humans makes it the most common sensory defect. Genetic etiology is the most common cause of sensorineural hearing loss (SNHL), with over 50% of congenital hearing loss attributed to genetic causes in the US (1). A total of 48 genes have been reported to be associated with autosomal dominant non-syndromic hearing loss (ADNSHL), one of those is the Purinergic Receptor P2X2 (*P2RX2*) (https://hereditaryhearingloss.org/).

Human *P2RX2* gene, located in 12q24.33, is composed of 10 exons (Gene ID: 22953). *P2RX2* encodes the P2X2 receptor, which is an ion channel purinoreceptor for adenosine triphosphate (ATP) that is broadly distributed in the mammalian tissues.

[†]Both laboratories contributed equally to this work.

Received: November 18, 2020. **Revised:** March 6, 2021. **Accepted:** March 12, 2021

P2X2 receptor assembles as trimers of the same subunits. Each unit has two transmembrane domains (TM1 and TM2), a large ectodomain and intracellular N- and C-termini (2). ATP activates P2X2 receptor by binding to extracellular pockets formed between the ectodomains of pairs of the three subunits. This drives a conformational change that leads to opening of a transmembrane ion permeation (3).

So far, three different deafness-related missense mutations in *P2RX2* were found, all leading to early-onset and progressive SNHL. *P2RX2* c. 1057G > C (p.Gly353Arg) was reported in an Italian family affected by ADNSHL (4). Age of onset was in the second decade of life and the severity of the disease seems to worsen with age. *P2RX2* c.601G > A (p.Asp273Tyr) was identified in a Japanese family suffering from severe SNHL and mitochondrial myopathy, encephalopathy, lactic acidosis and stroke-like episodes (MELAS) (5). Patients present progressive hearing loss beginning in their first or second decade of life. *P2RX2* c. 178G > T (p.V60L) mutation was identified in two unrelated Chinese families, as the cause of human DFNA41 form of dominantly inherited and progressive sensorineural HL (6). Affected family members were heterozygotes suffering from bilateral and early-onset hearing loss, with onset age ranging from 12-year-old to 20-year-old.

The *P2RX2* gene is highly conserved during evolution. Human and mouse *P2RX2* genes showed ∼77% identity at DNA and protein level (https://useast.ensembl.org). A *P2rx2* knockout (KO) mouse model was established and characterized, and it revealed P2X2 receptor playing an important role in regulating auditory neurotransmission in the inner ear (7), modulating vestibular function (8) and in sensory afferent signaling in multiple physiological systems (9). However, *P2rx2* KO mouse had normal hearing until 17-month-old (6), which was equivalent to human age of 50–60 years old (https://www.jax.org/news-and-insights/jax-blog/2017/november/when-are-mice-considered-old). Thus, *P2rx2* KO mouse model failed to mimic human patients for early-onset and progressive ADNSHL.

In order to understand the functional consequences of P2RX2 V60L, here we generated and characterized a knock-in mouse model based on human p.V60L mutation. The mutant animals showed early-onset of hearing loss at 21-day-old, and progressively lost their hearing capacity, being deaf at around 6-month-old, consistent with the patient clinical presentation. Molecular examination of the cochlea of mutant animals showed progressive abnormal morphology of the inner hair cells (IHCs) and spatial distribution of ribbon synapses, suggesting that *P2rx2* is essential for IHCs development and functionality. Our results showed that this could be the main mechanism for pathogenesis of deafness in this mouse model, and make it an excellent model to test future treatments.

Results

Generation and molecular characterization of *P2rx2* p.V61L knock-in mouse model

Human P2RX2 mutation in Val60 (NP_733782) is associated with DFNA41 (6). This aminoacidic is highly conserved between species (Supplementary Material, Fig. S1A). Mouse *P2rx2* gene is located on chromosome 5 and composed of 12 exons. In order to generate a mouse model carrying the syntenic amino acid change we perform a sequence alignment and identified the Val61 in the mouse P2rx2 protein (identifier: Q8K3P1-1) as the homolog to human Val60 (Supplementary Material, Fig. S1B). Mouse Val61 locates in an extremely conserved protein region and is encoded by GTC in mouse. We introduced a point mutation homologous to human *P2RX2* c. 178G > T (p.V60L), nucleotide site: chr12:133196029 G > T (hg19) on exon 2 of the mouse *P2rx2* gene, which changed mouse Val61 into Leu61. *P2rx2* mutant mice were generated by standard CRISPR-Cas9 protocols (10–12). The founder (G0) mice were genotyped, and one that contained the desired mutation in one allele was selected for establishing the colony. Segregation of both alleles and colony expansion was initially accomplished by breeding the G0 with wildtype (WT) CBA/J mice, to obtain heterozygous *P2rx2* c. 179G > C animals (from now on KI mouse). The mouse genotype was determined by Sanger Sequencing (Fig. 1A). During the process of expanding the colony we observed that pregnancy rates were different if the litters were coming for male or female KI mice. No litters were obtained when the male KI was paired with either WT or KI female (out of eight mating no litter was obtained), suggesting some male fertility problem that was not further studied within this work. Thus we never obtained homozygous KI mice. The animals analyzed in this manuscript came from the mating of Het KI females × WT males only (Supplementary Material, Fig. S3B).

In order to confirm the expression levels and the expected molecular weight of the P2rx2 WT and mutant proteins, western blot analysis using cerebellum derived protein extracts from 2-month-old WT or KI mice was performed. Both forms, WT and mutant P2rx2, were expressed and showed the expected molecular weight (Fig. 1B). To further assess the effect of *P2rx2* p.V61L mutation at the cellular level, we performed primary culture of mouse tail fibroblast from P15 WT and KI. During the cell culture process, we noticed KI fibroblasts line did not grow as fast as WT. Therefore, we performed Immunocytochemistry (ICC) to check subcellular localization, and cell ATP assay to check viability. In ICC, we used PMCA (membrane marker, red, Fig. 1C, Supplementary Material, Fig. S2A and B), 58 K Golgi (Golgi Apparatus marker, red, Supplementary Material, Fig. S2C and D) and ATP5A (mitochondria marker, red, Supplementary Material, Fig. S2E and F) to confirm the presence and subcellular localization of P2RX2 protein. P2RX2 was expressed in the plasma membrane, Golgi apparatus and mitochondria, which is consistent with previous reports (6,13,14). No obvious difference of P2RX2 subcellular localization was observed in WT and KI fibroblasts ICC (Supplementary Material, Fig. S2A–F). Next, we observed KI fibroblasts grew more slowly than WT. Thus, we performed ATP quantification for WT and KI fibroblasts, as a measure of viability. Total ATP was significantly reduced in KI compared with WT (luminescence reading for WT fibroblasts was 2523.83 ± 50.32, whereas for KI was 1979.58 ± 83.20; $P < 0.001$, Supplementary Material, Fig. S2G), suggesting a slower growth for KI derived cells.

To study the expression pattern of P2X2 receptors in the IE, we performed immunofluorescence on P0 or P1 WT and KI inner ear cross sections. P2RX2 was highly expressed in the organ of Corti, spiral ganglion and crista ampullaris of the lateral semicircular canal (Fig. 1D and E, Supplementary Material, Fig. S2H), in concordance with previous reports (7,8,15–17). P2X2 receptor (green) was highly expressed in the organ of Corti and spiral ganglion in P1 WT and KI derived cochlea (Fig. 1D and E). A high magnification of the organ of Corti, P2X2 receptor (green) expression is observed in inner and outer hair cells (OHCs) as well as in supporting cells. A high magnification on the spiral ganglion shows that spiral ganglion neurons (SGNs) were co-stained with P2X2 receptor and TUJ1 (red) indicating a strong expression on neurons. Interestingly, the localization of the WT and the mutant protein was similar, indicating that the mutation does not alter the spatial localization of P2rx2 in the IE (Fig. 1D and E). These

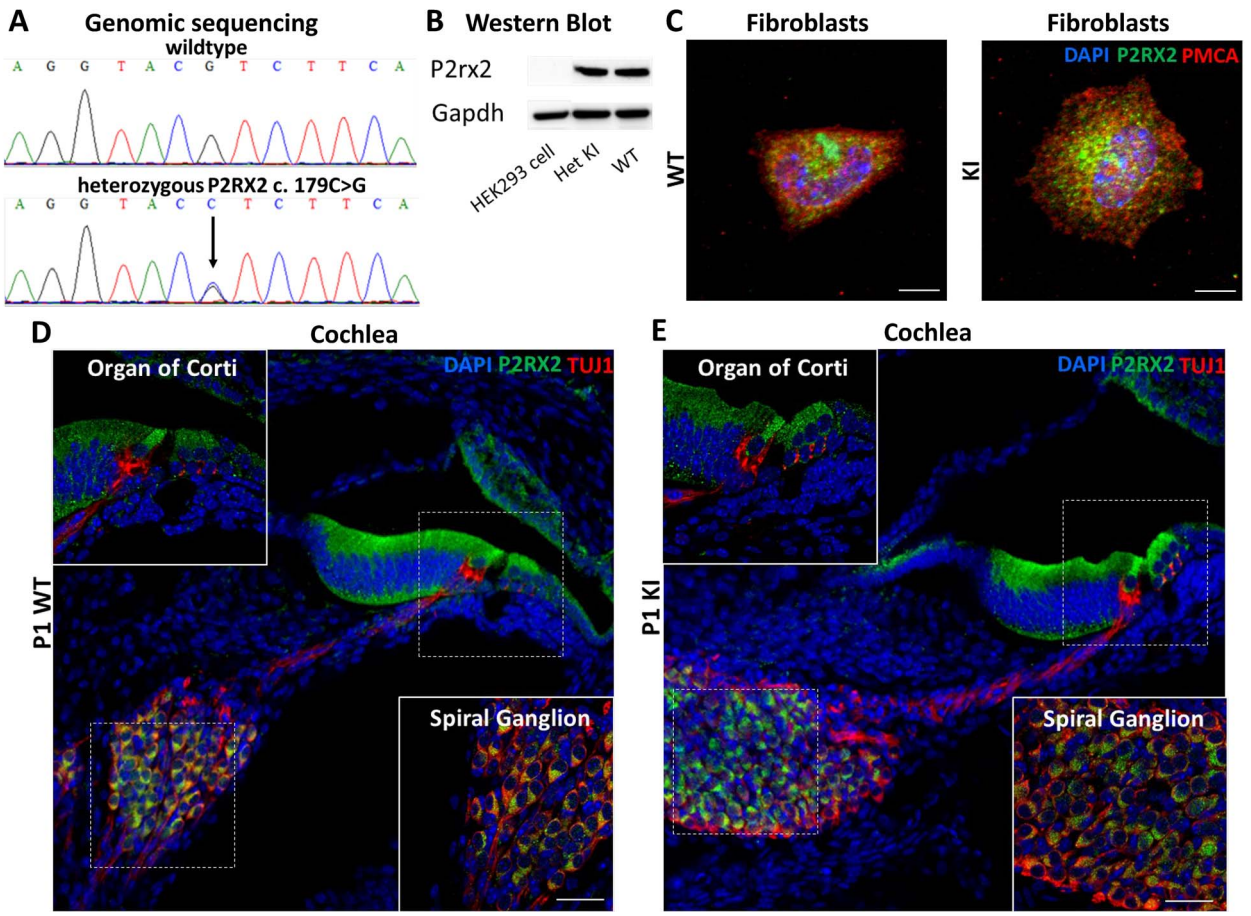

Figure 1. Molecular characterization of *P2rx2* c. 179G > C (p.V61L) mouse model. (**A**) Sanger sequence results of the heterozygous knock-in mouse model compared with WT. **G**TC was changed to **C**TC, demonstrating the missense mutation of mouse *P2rx2* c. 179G > C (p.V61L).(**B**) Western blot using mouse cerebellum cell's lysate showed P2rx2 protein presence in KI and WT mouse. HEK293 cells (Human Embryonic Kidney 293 cells) do not have endogenous *P2RX2*, therefore served as a negative control. Gapdh protein was detected on the same membrane after complete stripping, and used as internal control. (**C**) Immunostaining on fibroblasts cultured from P15 WT (left) and KI (right) mice tails. PMCA (cell membrane marker in red) and DAPI were used for nuclear staining (blue). P2RX2 (green) located on membrane in both lines, with no obvious subcellular localization difference. Scale bars = 10 µm. Localization of P2X2 receptor expression (green) in the P1 WT (**D**) or KI (**E**) mouse IE using immunofluorescence. TUJ1 (red) was used as neuronal markers and DAPI staining (blue) for nuclei. At high magnification on organ of Corti, P2X2 receptor (green) was expressed in IHC, OHC and supporting cells. Note the strong signal on the epithelial surface of these cells. At high magnification on spiral ganglion, most of SGNs were immunopositive for P2X2 receptor. Most P2X2 staining (green) was corresponding with TUJ1 (red) (E) P1 KI cross section showed no obvious difference from WT. P2X2 receptor was also highly expressed in organ of Corti and SGNs. Scale bars = 80 µm.

analyses confirmed the correct genetic modification and the expression of the mutated form. In addition, clary shows that *in vivo* the mutation does not alter the molecular weight, the subcellular localization or the IE expression pattern of the P2rx2 protein.

P2rx2 p.V61L knock-in mice exhibit normal general characteristics and activity level

No obvious changes in morphology or behavior (except for KI male fertility) were seen in *P2rx2* p.V61L knock-in mice (Supplementary Material, Fig. S3B). General characteristics were observed on 2-month-old male mice, including coat condition, piloerection, barbering, visual placing, vocalization while handling, vibrissae orienting, reaching response and full whiskers. No significant differences were observed between both genotypes regarding general characteristics, reflexes or body weight (WT = 26.30 ± 0.37 gr vs KI = 25.00 ± 0.72 gr; n = 11 for both groups, $P = 0.12$).

To measure locomotor activity, any presence of circular behavior and anxiety-like behavior, we conducted open field tests on 3-month-old male mice. KI mice did not show any significant difference from controls. Total distance traveled in 30 min session was 3011.99 ± 225.1 cm for WT (n = 10) and 3218.67 ± 557.5 cm for KI (n = 10, $P = 0.73$). Time spent in central zone/time spent in residue zone was 0.39 ± 0.04 for WT and 0.46 ± 0.04 for KI ($P = 0.21$). No circular behavior was observed for any genotype.

P2rx2 p.V61L knock-in mice mimic human patients' hearing loss

In order to assess hearing capabilities, we began testing KI and WT mice for ABRs and DPOAEs at 21-day-old. Interestingly, at this time, heterozygous KI mice exhibited mild hearing loss and gender differences. In ABR, male mice showed an ascending audiogram (worse hearing at high frequencies), whereas female showed a flat audiogram (worse hearing in low, mild and high frequencies), consistent with the gender difference in the pattern observed in affected human males that initially showed a sloping audiogram (high frequencies worse than low frequencies), whereas young affected human females typically had an ascending slope (high frequencies better than low frequencies) (18). 21-day-old WT mouse's

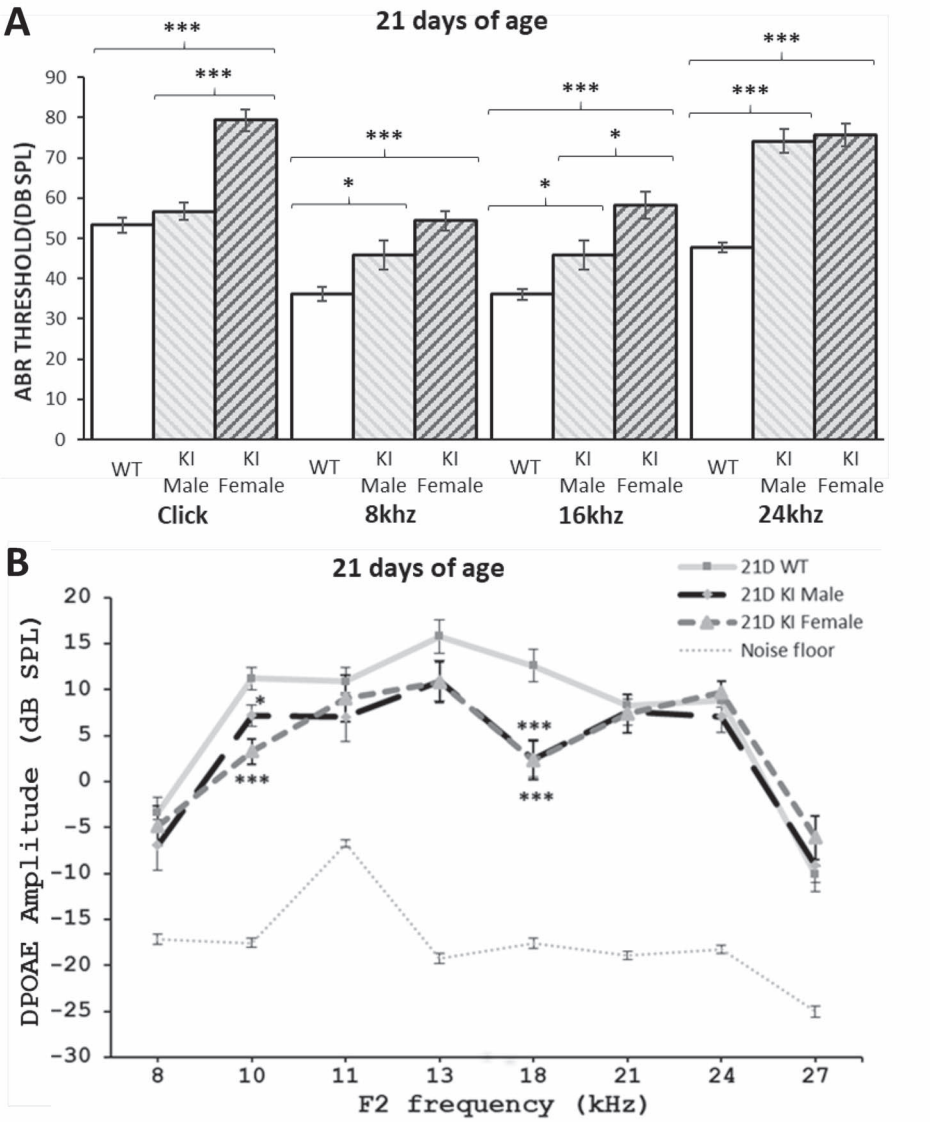

Figure 2. Gender difference in ABR and DPOAE for 21-day-old KI mice. (**A**) ABR assessment for 21-day-old WT (white columns) and KI (patterned columns) mice. KI female (black patterned columns) and male (grey patterned columns) significantly differed in click and 16 khz frequency. In contrast to WT, KI mice showed mild hearing loss at this age. (**B**) DPOAE amplitudes for eight frequencies (2f1 – f2) in 21-day-old WT (solid/top line) and KI (dotted/middle lines) mice. KI male (circles) displayed significantly elevated amplitudes than KI female (triangles) in F2 = 10 khz frequency (WT, n = 9; Male KI, n = 8; Female KI, n = 8; mean ± SEM). The corresponding noise background levels were plotted (dotted/bottom line). SPL, sound pressure level.

ABR thresholds at click, 8, 16 and 24 kHz were 53.33 ± 1.86, 36.11 ± 1.82, 36.11 ± 1.38 and 47.78 ± 1.21 dB SPL. 21-day-old female KI mouse's ABR thresholds at click, 8, 16 and 24 kHz were 79.3 ± 2.7, 54.3 ± 2.4, 58.1 ± 3.4 and 75.6 ± 2.9 dB SPL (n = 8/group, $P < 0.001$ at all tests), while males KI were 56.7 ± 2.1, 45.8 ± 3.7, 45.7 ± 3.7 and 74.2 ± 3.0 dB SPL (n = 8/group, $P = 0.26$, $P = 0.02$, $P = 0.01$, $P < 0.001$, respectively) (Fig. 2A). KI mice's ABR thresholds in females were significantly higher than those in males at click ($P < 0.001$) and 16 khz ($P = 0.033$). In DPOAE, 21-day-old female mice were significantly different from male at 10 khz ($P = 0.038$). DPOAEs at *F2* of 10 kHz in the female and male KI mice were 3.2 ± 1.3 and 7.1 ± 1.1 dB SPL, whereas WT was 11.2 ± 1.2 dB SPL (n = 8/group, $P < 0.001$, $P = 0.028$, compared to WT, respectively) (Fig. 2B).

We repeated hearing tests on KI and WT mice at ages of 2, 4 and 6 months. No significant difference was found between genders in mice older than 21 days thus both genders were analyzed together for older mice. In ABR, 2-month-old heterozygous KI mice exhibit bilateral and severe hearing loss at click, 8, 16 and 24 kHz (n = 14. 82.9 ± 3.6, 61.8 ± 4.1, 68.9 ± 3.7, 75.0 ± 3.2 dB SPL, respectively. $P < 0.001$ compared to age-matched WT for all frequencies tested). 4-month-old heterozygous KI mice's hearing became even worse (n = 13. 88.1 ± 2.3, 75.0 ± 3.7, 83.1 ± 2.2, 86.2 ± 3.5 dB SPL, respectively ($P < 0.001$ compared to age-matched WT for all frequencies tested. $P = 0.24$, $P = 0.026$, $P = 0.003$, $P = 0.027$ compared to 2-month-old KI, respectively) and indicated deafness (>80 dB SPL). When they were 6 months old, KI mice were deaf at click, 8, 16 and 24 kHz in ABR (n = 11. 93.6 ± 2.0, 77,7 ± 3.3, 84.1 ± 3.0, 88.2 ± 3.6 dB SPL, respectively. $P < 0.001$ compared to age-matched WT for all frequencies tested. $P < 0.001$ compared to 4-month-old KI for all frequencies tested (Fig. 3A–D). Just like human patients, heterozygous KI mice have early-onset and progressive hearing loss.

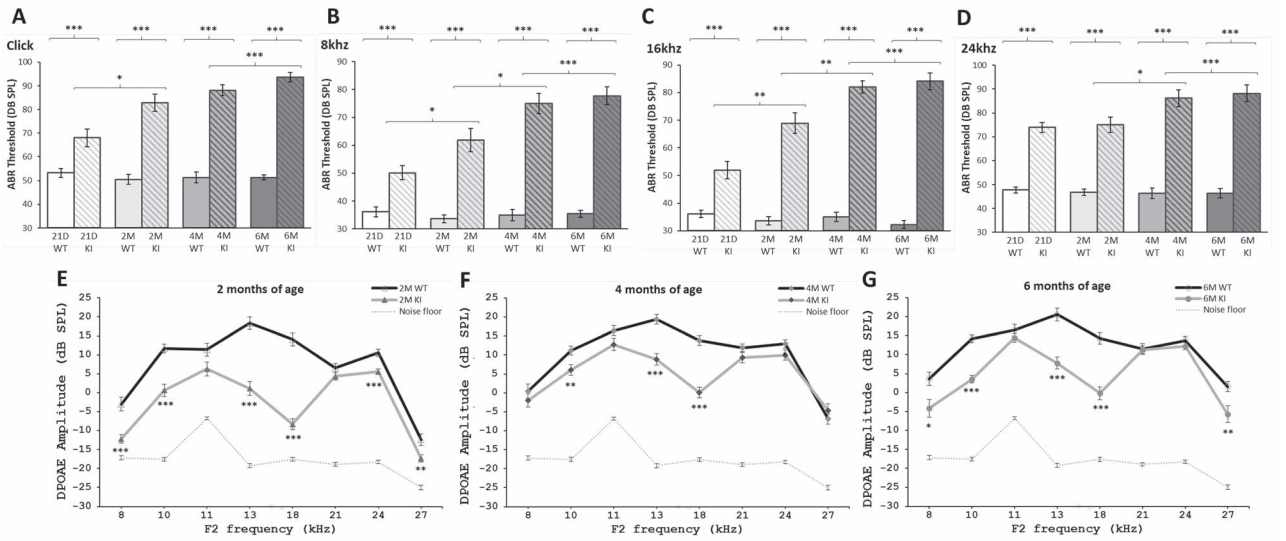

Figure 3. Progressive hearing loss in KI mice. **(A–D)** ABR thresholds measured in WT (solid columns) and *P2rx2* p.V61L knock-in (patterned columns) mice at age of 21 days, 2 months, 4 months and 6 months in click-evoked and pure tones stimuli. ABR thresholds were increased in KI mice progressively with age, from mild hearing loss to deafness across all frequencies (click, 8, 16, 24 khz). 21-day-old female and male were combined here to show progression of hearing loss. **(E–G)** DPOAE amplitudes measured in WT (black/top line) and KI (grey/middle line) mice aged 2, 4 and 6 months, including the mean noise floor across the testing frequencies (dotted/bottom line). KI mice showed significantly reduced DPOAE thresholds at *F2* = 10, 13 and 18 kHz in all age groups (21D WT, n = 9, 21D KI, n = 16; 2 M WT, n = 11; 2 M KI, n = 14; 4 M WT, n = 11; 4 M KI, n = 13; 6 M WT, n = 11; 6 M KI, n = 11. mean ± SEM).

In addition, DPOAE in KI mouse was significantly reduced in certain low, middle and high frequencies at ages of 2, 4 and 6 months (Fig. 3E–G). In comparison with same age WT mice, DPOAEs in 2-month-old KI mice at *F2* = 8, 10, 13,18, 24 and 27 kHz were significantly reduced by −9.19 ± 0.92, −11.07 ± 0.77, −17.23 ± 0.61, −22.37 ± 0.94, −5.09 ± 0.91 and − 4.98 ± 0.76 dB SPL, respectively ($P < 0.001$ at all frequencies). 4-month-old KI displayed significantly lower DPOAE amplitude than WT at F2 = 10,13 and 18 kHz ($P = 0.009$, $P < 0.001$, $P < 0.001$, respectively). 6-month-old KI mouse continued to show reduced amplitude, recorded data was significantly lower than WT at F2 = 8, 10, 13, 18, 27 kHz ($P = 0.01$, $P < 0.001$, $P < 0.001$, $P < 0.001$, $P = 0.007$, respectively). Impaired ABRs and reduced DPOAE amplitudes shown in KI mouse indicates auditory neuropathy.

P2rx2 p.V61L knock-in mice exhibit vestibular disfunction and pain hypersensitivity

To investigate the vestibular function of the mutant mice, we performed the rotarod tests on 2-month-old males and the beam crossing tests on 3-month-old on males of both genotypes. In accelerating rotarod test, mice received three rotarod trials per day for three successive days. Mice were allowed to stay on the rotarod for a maximum of 300 s per trial. Shorter latencies to fall were observed in *P2rx2* p.V61L mice in every nine trial (n = 11 each group, 84.91 ± 9.35 vs 15.55 ± 4.58, 83.27 ± 15.21 vs 35.09 ± 9.46, 113.91 ± 16.70 vs 39.27 ± 9.01, 177.63 ± 22.43 vs 63.64 ± 7.29, 206.82 ± 21.73 vs 82.09 ± 14.54, 239.45 ± 21.57 vs 107.08 ± 8.39, 228.73 ± 22.27 vs 72.55 ± 10.01, 240.36 ± 22.28 vs 106.36 ± 8.41, 268.00 ± 12.81 vs 132.55 ± 17.07, respectively. $P < 0.001$, $P = 0.014$, $P < 0.001$, $P < 0.001$, $P < 0.001$, $P < 0.001$, $P < 0.001$, $P = 0.005$, $P = 0.008$, respectively) (Fig. 4A). Both groups demonstrated typical learning. Consistently, impairment of motor coordination and balance was also observed in *P2rx2* p.V61L knock-in mice in the beam walking test, in which it took significantly longer for KI mice (WT n = 15, 28.40 ± 10.34 vs KI n = 11, 79.10 ± 6.34. $P < 0.001$, Fig. 4B) to arrive and harder to complete the task (WT n = 15, 1.90 ± 0.43 vs KI n = 11, 0.30 ± 0.15. $P = 0.002$, Fig. 4C).

As it is possible that the motor deficits displayed by the KI mice could be due to general muscle weakness, we measured grip strength at the age of 3 months old and found no significant difference in either forelimb (n = 10 for each group. $P = 0.28$) or hind-limb (n = 10 for each group. $P = 0.81$) strength between the two genotypes (Supplementary Material, Fig. S3B). Taken together these data suggest a vestibular dysfunction in KI mice.

Based on the clear link of P2RX2 with the sensory system, we conducted hot plate tests to measure the nociceptive response in the KI mice. Latencies to show nociceptive behaviors (first paw lick) on the hot plate significantly differed between WT and KI mice (n = 11, 10.75 ± 0.39 vs 9.45 ± 0.17. $P = 0.007$, Fig. 4D), which suggested KI mouse were more sensitive to pain than wildtype.

P2rx2 p.V61L knock-in mice exhibit normal cochlear structure

Based on our hearing tests findings that *P2rx2* p.V61L knock-in mice displayed early-onset and progressive hearing loss, we subsequently assessed cochlear morphology. First, we stained P2 mice's cochlear with DAPI (nuclei marker, blue), Myo7a (hair cell marker, red) and phalloidin (stereocilia marker, green) (Fig. 5A). Both WT and KI exhibited normal organ of Corti structure, including three rows of OHCs, one row of IHCs and V-shaped stereocilia on every hair cell. There was no obvious loss of hair cells or stereocilia, and it retained the normal shape. We continued the histological investigation in P25 mice using the same staining technique except replacing phalloidin with P2RX2 (green) (Fig. 5B). There was no obvious hair cell loss in P25 KI mouse. Interestingly, we noted that P2RX2 staining was intense in the basal pole of IHCs and olivocochlear terminals of inner spiral bundles in the IHC area, which is normally the localization of synapsis (19). Moreover, P2RX2 has been reported to be expressed in postsynaptic junctions in IHCs and OHCs (17).

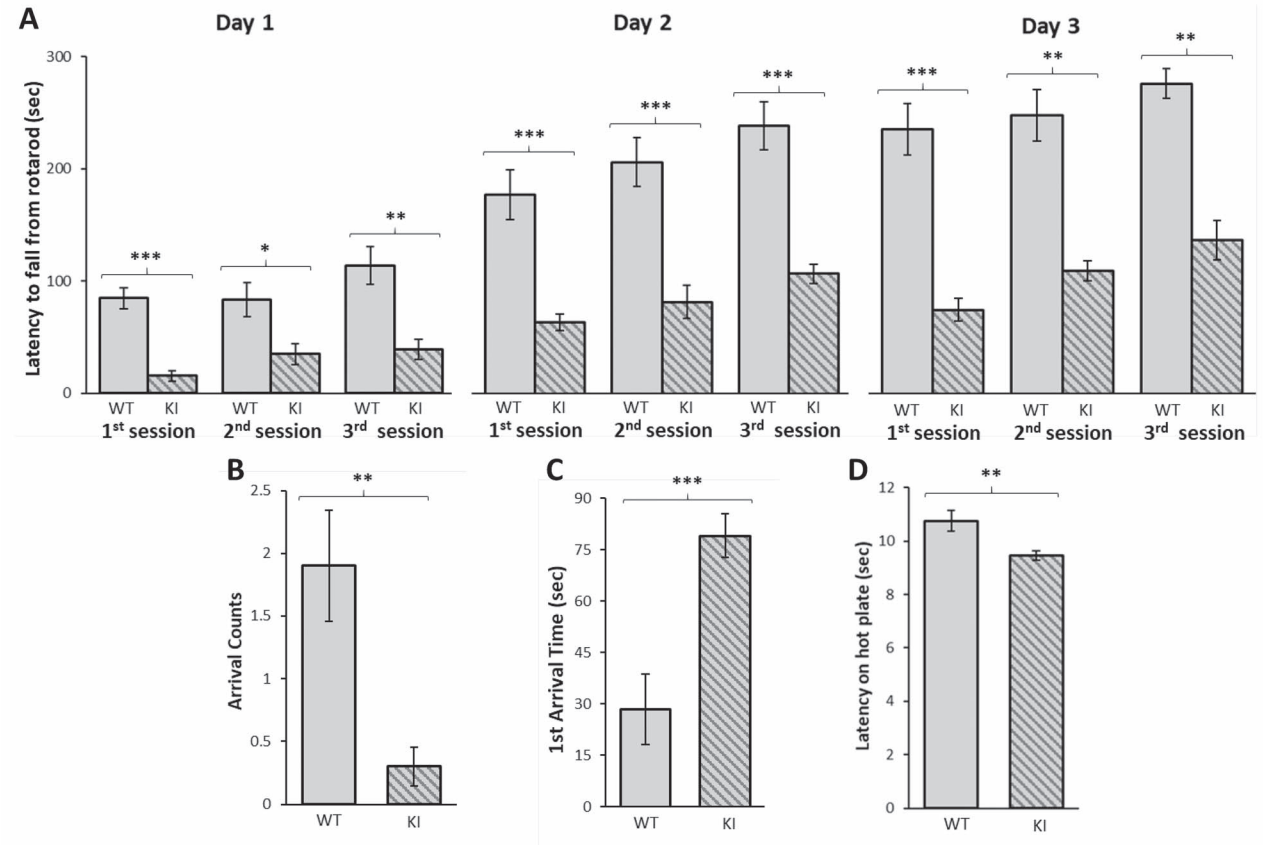

Figure 4. Vestibular dysfunction and pain hypersensitivity in KI mice. (**A**) Rotarod tests revealing significantly decreased latencies for KI (patterned columns) in every trial compared to WT (grey columns), which indicated vestibular dysfunction. (**B-C**) Beam crossing test revealing it was harder for KI mice (patterned column) to cross the beam than WT (grey column), which further demonstrated vestibular disfunction for KI mice (WT, n = 15; KI, n = 11. mean ± SEM). (**D**) Hot plate test revealing decreased latency to pain in KI mice (patterned column), which agreed with previous studies showing P2X2 receptor's role in sensory afferent signaling (WT, n = 11; KI, n = 11. mean ± SEM).

This led us to investigate further with synapse distribution in KI mouse.

P2rx2 p.V61L knock-in mice display aberrant distribution of synaptic ribbons and IHC degeneration without hair cell loss

To understand the role of *P2rx2 V61L* in inner-ear development and function, we expanded our assessment to IHC-afferent fiber synapses. We performed immunostaining on P2, 1-month-old and 4-month-old mice's cochlea. CtBP2 (red) was used to stain synaptic ribbons, which also faithfully labeled nuclei. Myosin VIIa (blue) was used to stain the hair cell body (Fig. 6A–C). Analysis of the synapses in cochlear tissues confirmed that *P2rx2 V61L* produced no OHC or IHC loss. From ages of P2 to 4 months, KI showed three straight rows of OHCs and one line of IHCs. No obvious hair cell loss was observed. At the age of P2, the presynaptic ribbons located evenly all over the IHCs in WT and KI (Fig. 6A). The total number of CtBP2 puncta was counted in each z-stack and was divided by the number of IHCs (n = 100 IHCs from two experiments). WT and KI displayed similar numbers of ribbons per IHC (21.55 ± 0.33, 20.72 ± 0.33, respectively, $P = 0.08$). In normal matured mouse cochlea, all ribbons (CtBP2-labeled, red) were located along the IHC's basolateral membrane (20). However, 1-month-old KI mice's cochlea exhibited abnormal localization of synaptic ribbons in IHCs. Apparently, CtBP2 puncta moved apically to the perinuclear area (Fig. 6B). In 4-month-old KI, the abnormal distribution of ribbons became visually more progressive. Synapses located close to the IHC nuclei, whereas in WT mice, all ribbons were distributed far away from the nuclei (Fig. 6C). At individual IHCs, there was no significant difference of ribbons quantification in 1-month-old mouse (17.16 ± 0.30 vs 17.73 ± 0.23, $P = 0.14$). However, in 4-month-old mouse, KI had significantly more ribbons than WT. There were 12.41 ± 0.19 CtBP2 puncta per IHC in WT and 16.93 ± 0.16 in KI ($P < 0.001$) (Fig. 6D). Abnormal morphology of IHCs was also observed visually in 1-month-old and 4-month-old KI mouse. Measurement of IHC length in z-stack confirmed the morphologic change (n = 100 IHCs from two experiments) (Fig. 6E). There was no significant difference of IHC length at age of P2 between WT and KI (11.67 ± 0.16 um vs 11.63 ± 0.22 um, $P = 0.90$). However, at the age of 1 month, IHC length was 26.68 ± 0.21 μm in WT ($P < 0.001$ compared to P2 WT) and 21.47 ± 0.15 μm in KI ($P < 0.001$ compared to age-matched WT, $P < 0.001$ compared to P2 KI). At the age of 4 months, WT's IHC continued the elongation compared with 1-month WT (31.02 ± 0.29 μm, $P < 0.001$), whereas KI remained about the same as 1-month (21.23 ± 0.30 um. $P = 0.46$ for 1 month and 4 months KI. $P < 0.001$ for age-matched WT). The shorter length of IHC in KI suggests that *P2rx2 V61L* is involved in the maturation of IHC. The progression of aberrant distribution of synaptic ribbons and IHC abnormal maturation observed in KI mouse could affect auditory function, which may be consistent with the progression of hearing loss.

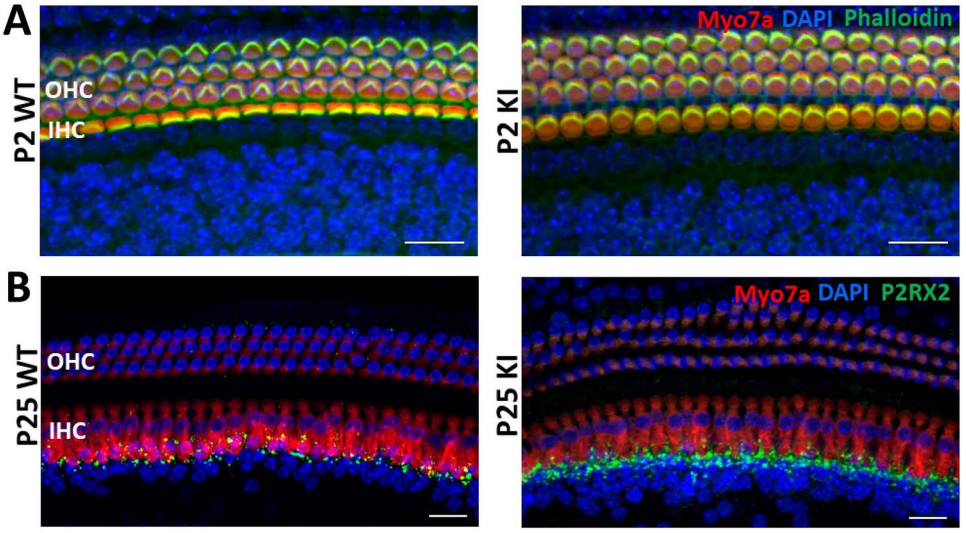

Figure 5. Immunofluorescence analysis of WT and KI mice whole-mount inner ears' middle turn structure at the age of P2 and P25. (**A**) Representative hair cells images of P2 WT and KI mice. Myosin VIIa was marker for hair cell (red). DAPI was marker for nuclei (blue). Phalloidin was marker for stereocilia (green). P2 KI(right) showed three rows of OHCs and one row of IHC, just like WT(left). There was typical shaped stereocilia on each hair cell in KI mice. (**B**) Representative images of P25 mice stained with Myo7a (red), DAPI (blue) and P2RX2 (green). No obvious difference was observed in KI. Noted strong P2RX2 labeling in basal pole of IHC and dendritic terminals area. Scale bars = 20 μm.

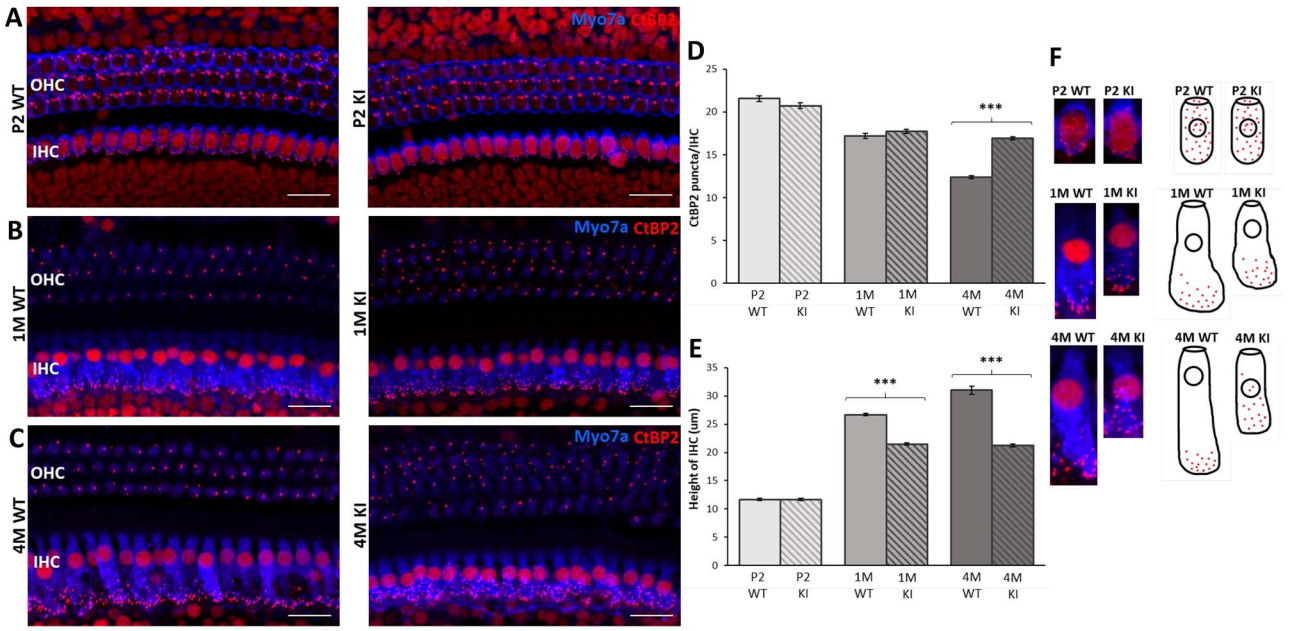

Figure 6. Progressive ribbon and IHC degeneration in KI mice. (**A–C**) Representative confocal image of Myo7a (blue) and CtBP2 (red, marker for synaptic ribbon) staining in middle turn of P2, 1-month-old and 4-month-old mice. No obvious hair cell loss was observed. KI(right) IHCs showed progressively abnormal morphology with irregular pattern of synaptic ribbons distribution. In adult WT (left), ribbons were located in the basal pole of IHC. But in adult KI, some ribbons were dislocated to IHC nuclei area. Scale bars = 20 μm. (**D**) CtBP2 puncta quantification of WT (solid columns) and KI (patterned columns) in each age group using z-stack. There was no statistic difference in P2 and 1 month. 4-month-old KI had significantly more ribbons than WT. (**E**) Height measurements of IHCs in middle turn of the cochlea revealing IHCs were progressively shortened in KI (patterned columns) compared to WT (solid columns). (**F**) Single IHC cropped from Figure 6A–C and schematic diagram of IHCs demonstrating the progression of IHC morphology change in KI mice.

Discussion

Here, we present the generation and characterization of a novel hearing loss mouse model obtained by Crisper/Cas technology. To the best of our knowledge, our model is the first knock-in mouse harboring *P2RX2* c. 178G > T (p.V60L) known to cause ADNSHL in human patients. The characterization of the *P2rx2* p.V61L knock-in mouse reveals that it faithfully reproduces what is expected based on the human phenotype: early-onset, bilateral, dominantly inherited, progressive and sensorineural HL with gender difference at onset. Moreover, *P2rx2* p.V61L knock-in mouse model exhibits vestibular dysfunction and increased sensitivity to pain. We examined KI mice's cochlear structure and

found progressive IHC degeneration with relocation of ribbon synapses, which could lead to hearing loss.

In mature hearing mammals, most of the cochlear output relies on IHCs. 95% of the auditory afferent neurons communicate with IHCs through synapsis and type I afferents, which locate on IHCs' basolateral aspect. A single IHC makes synaptic contact with 5 to 30 SGNs. However, each SGN contacts a single IHC via a single ribbon synapse (21). In contrast, OHCs receive the residual 5% via type II afferents (22). Therefore, cochlear IHC ribbon synapses play an important role in sound encoding and neurotransmitter release. Synaptic ribbons locate on neural terminals closer to the IHC basal poles in adult human and mouse. The IHC ribbon synapses are the first afferent synaptic connection in the hearing pathway, and they transmit acoustic information from IHCs to the terminals of SGNs (23). Each IHC ribbon synapse is the sole input to one SGN. The main structural components of the ribbon are ribeye/CtBP2. Ribbon release neurotransmitters when it is induced through periodic excitation of IHCs (24), resulting in IHC Ca2+ spikes, glutamate release and ultimately bursts of action potentials in SGNs that are carried to the brain by auditory nerve fibers (25). IHC Ribbon synapses are essential for hearing. Each synapse having one presynaptic ribbon and release site onto one afferent, and then communicate to one SGN. Proper positioning of ribbon synapses, which undergoes complex organizational processes during the maturation of IHC, is required for normal hearing (26). The relocation of ribbons from the IHC basal pole to the IHC bundle pole has been reported as the cause of hearing loss, with or without hair cell loss, with or without reduced number of ribbons (23,27–31). Here, we found a pattern of degenerated ribbons in KI mice IHCs, which were located closer to nuclei than WT. IHC defects, including the degenerated synapses, may be secondary to other underlying mechanisms. Interestingly, the number of ribbons in KI remained similar to WT at age of P2 and 1 month, then became more than WT at 4 months. There are reports demonstrating ribbons number restored naturally without hearing recovery in noise-induced and drug-induced hearing loss mice model (28,29,32). So Cochlear ribbon synapses have intrinsic capacity to spontaneously regenerate (33). However, affected SGNS are hardly recovered from noise damage and ototoxic drugs (34,35). In our case the permanent 'silenced' SGNs may contribute to *P2rx2* KI mice's progressive hearing loss.

Numerous studies have characterized *P2rx2* knockout mouse model which interestingly differed from our knock-in mouse. Comparing characterizations between knockout and knock-in mouse model reveals that our *P2rx2* p.V61L knock-in mouse is a better model for investigating hearing loss and neurological disease (Table 1). *P2rx2* KO mice were from background strain C57BL/6 J. *P2rx2* KI mice were from CBA/J strain. Both strains are commonly used for transgenic mouse line development and hearing-related studies. Background strain may contribute to the phenotype difference. *P2rx2* KO mice started hearing loss at the age of 17 months (6), whereas our knock-in mice exhibited mild hearing loss at 21-day-old and progressively become deaf at 4-month-old. Early-onset hearing loss makes our knock-in mouse model a better tool for future studies of drug treatment and genetic rescue. In terms of general sensory function and motor coordination as assessed by a neurological evaluation that included the Irwin test, visual cliff, hot plate test, grip strength, balance beam and rotarod test, *P2rx2* KO mice showed no difference from WT (9). The abnormal parameters among a series of neurological assessment tests for *P2rx2*-null mice were the decreased vestibulo-ocular reflex (VOR) response and balance impairment on beam crossing (8). The *P2rx2* p.V61L knock-in mouse model generated and described in this work exhibited neurological dysfunction in hot plate, rotarod and beam crossing tests as well as a progressive hearing loss, recapitulating the human phenotype hence making it a better system to understand the mechanisms underlying the clinical presentation and to study possible therapies.

Computer three-dimensional modeling suggested V60L mutation can result in altered conformational changes, leading to inability of human P2RX2 channel to bind ATP (36). Consistently, biophysical study revealed that V60L dominant mutant formed conductive channels but were insensitive to ATP, which suggest that the mutant functionally uncouples the pore from the ATP binding sites in the extracellular domain (14). Moreover, it has been reported that V60L dominant deafness mutation do not have negative effects on WT P2X2 isoforms (13). Thus, we speculate the hearing loss in our V61L heterozygous KI mice was caused by conformational changes of P2X2 receptor, which resulted in IHCs defects. And there are other underlying mechanisms that regulate V61L and WT isoforms function. This speculation needs to be further investigated in the future, including crossing KI with KO mice and performing electrophysiology on hair cells.

Materias and Methods

Animals

The *P2RX2* gene is highly conserved during evolution, showing ~77% identity at DNA and protein level (Supplementary Material, Fig. S1A), making the mouse an excellent model for this mutation.

P2rx2 mutant mice were generated by CRISPR-Cas9 technology at the Mouse Genome Engineering Core Facility, University of Nebraska Medical Center. The CBA/J strain (Jackson laboratories stock number 000656) was used as the background to develop the model. CRISPR-Cas9 protocols were followed as described previously (10–12). Briefly, CRISPR Ribonucleoprotein complex consisting of Cas9 protein, a guide RNA GCACGATGAAGACGTACCTG (that cleaves at four bases upstream of the desired mutation site) and the donor oligonucleotide to convert Valine (**G**TC) to Leucine (**C**TC) were injected into CBA/J zygotes and the microinjected zygotes were transferred into pseudo-pregnant females. The genomic region from the founder mice were amplified using PCR primers P2XR2 F- CTTTACTTCGTGTGGTGCGCCG and P2XR2 R-CACGTCCCACACTTTGTGTTC and the mutation was confirmed by sequencing and restriction fragment length polymorphism (RFLP) using *KpnI* Restriction Enzyme (expected band sizes: wild type; 270 bp, homozygous mutant; 157 bp +113 bp, Heterozygous mutant; 157 bp + 113 bp + 270 bp). A founder mouse carrying a *P2rx2* c. 179G > C (p.V61L) was used for colony expansion by breading with wildtype (WT) CBA/J mice. The mice were housed in groups of two to five per cage and allowed free access to food and water. The animals were maintained under standard conditions (room temperature: 22 ± 2°C; relative humidity: 55 ± 10%) on a light:dark cycle of 12:12 h (6:00 a.m. to 6:00 p.m.). All procedures were approved by the University of Miami Institutional Animal Care and followed the National Institutes of Health (NIH) Guidelines, 'Using Animals in Intramural Research'.

All mice were weaned at 21-day-old, at which time a 1–2 mm end-of-tail clip sample was collected for genotyping. Genomic DNA was extracted, and each mouse's genotype was determined by a commercial DNA sequencing service (Genewiz, Inc.).

One batch of WT and KI mice were used for a series of tests including general characteristics, rotarod, grip strength, ABR and

Table 1. Characterization of P2rx2 KO mouse model vs P2rx2 p.V61L KI mouse model

	P2rx2 KO mouse model	*P2rx2* p.V61L KI mouse model
General characteristic	normal	normal
Open field	normal	normal
Hearing loss	onset at 17-month-old	onset at 21-day-old and progression
Rotarod	normal	abnormal
Hot plate	normal	abnormal
Male fertility	abnormal	abnormal

DPOAE, beam crossing, open field and hot plate. The other batch was used only for ABR and DPOAE at 21-day-old. The number of mice (n) utilized is mentioned in each experiment. The order and timeline of the battery of tests is represented in Supplementary Material, Figure S3A. On testing day, mice were kept in their home cages and acclimate to the testing room for at least 30 min.

Neuromuscular, nociception and vestibular function testing

Rotarod: Animals were placed on the rotarod (Med Associates) where the rod accelerates from 4 to 40 rpm. The latency to fall was recorded. The test was done three times a day (first session, second session and third session) for three consecutive days (Day 1–3) and had a 15 min resting period between sessions.

Open field: Animals were placed individually in the center of an open-field box (40 cm × 40 cm × 30 cm; Med Associates), and their spontaneous motor activity was recorded for 30 min. The computer program automatically recorded the following parameters: distance traveled, zone entries, ambulatory counts, stereotypic counts, vertical counts and time spent in predefined zones.

Beam crossing: The balance beam task was used to assess balance and fine motor coordination. Mice were positioned on the center of a 50 cm long and 1 cm wide wooden bar, which is attached to two support columns 44 cm above a padded surface. At both ends of the bar, 9 cm × 15 cm wooden escape platforms were installed. Each mouse was first given training then a test in the same day. The time each animal remained on the beam was recorded. The total testing time was 90 s.

Grip strength: Neuromuscular abilities and muscle strength were measured by grip strength. After the animals were placed on an electronic grip strength meter (Model: BIO-GS3), their forelimbs strength was measured first then the whole limbs. The mice were gently grasped at the base of their tails to determine their highest grip strength. The measurements were repeated two times with 1 min rest between trials. The maximal readings were recorded.

Hot plate: The hot plate test was used to evaluate nociception or sensitivity to a painful stimulus. Mice were placed on a hot plate machine (Stoelting Co.) at 55.0°C ± 1°C. The time to the first sign of nociception, paw licking or jump response was recorded and the animal immediately removed from the hot plate. A cut-off period of 20 s was maintained to avoid damage to the paws.

Hearing tests

To assess hearing capabilities, auditory brainstem responses (ABRs) and distortion product optoacoustic emissions (DPOAEs) were recorded and analyzed. Each animal was anesthetized with an intraperitoneal injection of a mix of ketamine/xylazine (120/10 mg/kg body weight) prior to testing. Using a heating pad, the body temperature of the mice was kept at 37°C for the duration of the test and the recovery period. DPOAEs were measured and recorded first followed by the ABRs. Both tests were conducted using a Smart EP Universal Smart Box (Intelligent Hearing Systems, Miami, FL). The threshold for ABR was defined as the lowest stimulus level at which a repeatable morphology could be identified in the response waveform. The threshold for DPOAEs was defined as the F1 level required to produce a response amplitude of 0 dB SPL.

Western blot

The cerebellum tissues were lysed with RIPA lysis buffer containing protease and phosphatase inhibitors 100 µM on an ice box. The cerebellum homogenates were centrifuged in a centrifugal machine for 15 min 12 500 rpm, 4°C, and the supernatants were collected in an independent tube. HEK293 cells were lysed after 48 h of transfection. Subsequently, 40 µg of the total protein from each sample was transferred onto PVDF membranes 0.45 µm, blocked with 5% milk, and incubated with primary antibody P2rx2 (Novus, USA) overnight at 4°C, followed by HRP-conjugated secondary antibody goat anti-rabbit (Cell Signaling Technology, USA) at room temperature for 1 h. Chemiluminescence detection and imaging system were used to capture and analyze the protein bands. Using Stripping Buffer (Thermo Fisher Scientific, USA) to wash off P2rx2 bands, then blocked for 1 h and incubating the same membrane with primary antibody Gapdh (Cell Signaling Technology, USA); then incubating with HRP-conjugated secondary antibody goat anti-rabbit (Cell Signaling Technology, USA).

Mouse tail fibroblast primary culture

P15 mice's tails were cut 0.5–1.0 cm from tip with sterile scissors and placed in a cell culture dish containing RPMI media. Over time, the fibroblasts migrated out of the tissue onto the surface of the dish. Excess tissue was removed. Following extraction, the fibroblasts were cultured in RPMI with antibiotics. Two cell lines, WT and KI, were maintained in 5% CO2 incubator at 37°C.

Viability assay

CellTiter-Glo Luminescence Assay (Promega Corporation, USA) was used to test ATP level in WT and KI fibroblasts cell line as a proxy for viable cells remaining in a 24 h culture. Cells were seeded at 2000 cells/well in a 96-well plate; six independent experiments were done. ATP disodium salt (Sigma, USA) was prepared as standards to generate ATP standard curve. After adding CellTiter-Glo reagents, fibroblasts and standards were measured in the same 96-well plate using Synergy™2 Multi-Mode Microplate Reader (Biotek, USA).

Immunofluorescence

Inner ears from P0 and P1 WT and KI mice were fixed with 4% (vol/vol) paraformaldehyde (PFA) for at 4°C overnight. The cross sections were blocked and incubated overnight with primary antibody in PBS. A mouse anti-Tubulin β 3 (TUBB3) monoclonal antibody (TUJ1-801201, BioLegend, USA) and a rabbit anti-P2RX2 polyclonal antibody (NBP2-19655, Novus, USA) were utilized as primary antibodies. Co-staining was performed with DAPI (Calbiochem, San Diego, CA).

Whole cochleae were dissected from mice and immediately were fixed in 4% PFA/PBS overnight at 4°C. Middle turns were then dissected and the treated with a blocking buffer (PBS with 5% BSA and 0.1% Triton X-100) for 1–3 h at room temperature and immunostained with mouse anti-Myo7a monoclonal antibody (138-1, Developmental Studies Hybridoma Bank, USA) and rabbit anti-P2RX2 polyclonal antibody (NBP2-19655, Novus, USA). Then probed with Alexa Fluor 488 phalloidin (A12379, Thermo Fisher, USA). Another batch of whole cochleae tissue sample was immunostained with (1) mouse anti-CtBP2 antibody (612 044, BD Biosciences, USA) at 1:200; (2) rabbit anti-Myo7a antibody (sc-25 834, Santa Cruz, USA) at 1:100. Appropriate secondary antibodies coupled to Alexa Fluor were used in the red and blue channels.

Fibroblast cultured from P15 mice tail were fixed and blocked the same way as the method above. Then immunostained overnight at 4°C with rabbit anti-P2RX2 polyclonal antibody (NBP2-19655, Novus, USA), mouse anti-PMCA ATPase monoclonal antibody (MA3-914, Thermo Fisher, USA) and mouse anti-ATP5A monoclonal antibody (ab14748, Abcam, USA), or mouse anti-58 K Golgi monoclonal antibody (NB600-412, Novus, USA). Next day DAPI (Calbiochem, San Diego, CA) and secondary antibody couples to Alexa Fluor was used for co-staining. Signals were visualized on a Zeiss LSM710 laser confocal microscope. The Z stacks of the confocal images were exported to ImageJ and fluorescence intensity was analyzed in ImageJ utilizing the same settings for all the samples.

Statistical analysis

Statistical analysis was performed by Microsoft Office Excel 2016 using one-way ANOVA. Data are expressed as mean ± SEM. *P*-values <0.05 were considered statistically significant. Chi-square test was used to calculate statistical significance for fertility. All sample size and *P*-values were reported in the figures or the figure legends. Asterisks were given as following, $^{*}P < 0.05$; $^{**}P < 0.01$; $^{***}P < 0.001$.

Supplementary Material

Supplementary Material is available at *HMG* online.

Acknowledgements

This study was supported by NIH grants of R01DC005575 and R01DC012115 to X.Z.L.

Conflict of Interest statement. The authors have no conflicts of interest to declare.

References

1. Morton, C.C. and Nance, W.E. (2006) Newborn hearing screening–a silent revolution. *N. Engl. J. Med.*, **354**, 2151–2164.
2. Mittal, R., Chan, B., Grati, M., Mittal, J., Patel, K., Debs, L.H., Patel, A.P., Yan, D., Chapagain, P. and Liu, X.Z. (2016) Molecular structure and regulation of P2X receptors with a special emphasis on the role of P2X2 in the auditory system. *J. Cell. Physiol.*, **231**, 1656–1670.
3. Stelmashenko, O., Compan, V., Browne, L.E. and North, R.A. (2014) Ectodomain movements of an ATP-gated ion channel (P2X2 receptor) probed by disulfide locking. *J. Biol. Chem.*, **289**, 9909–9917.
4. Faletra, F., Girotto, G., D'Adamo, A.P., Vozzi, D., Morgan, A. and Gasparini, P. (2014) A novel P2RX2 mutation in an Italian family affected by autosomal dominant nonsyndromic hearing loss. *Gene*, **534**, 236–239.
5. Moteki, H., Azaiez, H., Booth, K.T., Hattori, M., Sato, A., Sato, Y., Motobayashi, M., Sloan, C.M., Kolbe, D.L., Shearer, A.E. *et al.* (2015) Hearing loss caused by a P2RX2 mutation identified in a MELAS family with a coexisting mitochondrial 3243AG mutation. *Ann. Otol. Rhinol.Laryngol*, **124**, 177S–183S.
6. Yan, D., Zhu, Y., Walsh, T., Xie, D., Yuan, H., Sirmaci, A., Fujikawa, T., Wong, A.C., Loh, T.L., Du, L. *et al.* (2013) Mutation of the ATP-gated P2X(2) receptor leads to progressive hearing loss and increased susceptibility to noise. *Proc. Natl. Acad.Sci.U.S.A*, **110**, 2228–2233.
7. Housley, G.D., Morton-Jones, R., Vlajkovic, S.M., Telang, R.S., Paramananthasivam, V., Tadros, S.F., Wong, A.C., Froud, K.E., Cederholm, J.M., Sivakumaran, Y. *et al.* (2013) ATP-gated ion channels mediate adaptation to elevated sound levels. *Proc. Natl. Acad.Sci.U.S.A*, **110**, 7494–7499.
8. Takimoto, Y., Ishida, Y., Kondo, M., Imai, T., Hanada, Y., Ozono, Y., Kamakura, T., Inohara, H. and Shimada, S. (2018) P2X2 receptor deficiency in mouse vestibular end organs attenuates vestibular function. *Neuroscience*, **386**, 41–50.
9. Cockayne, D.A., Dunn, P.M., Zhong, Y., Rong, W., Hamilton, S.G., Knight, G.E., Ruan, H.Z., Ma, B., Yip, P., Nunn, P. *et al.* (2005) P2X2 knockout mice and P2X2/P2X3 double knockout mice reveal a role for the P2X2 receptor subunit in mediating multiple sensory effects of ATP. *J. Physiol.*, **567**, 621–639.
10. Harms, D.W., Quadros, R.M., Seruggia, D., Ohtsuka, M., Takahashi, G., Montoliu, L. and Gurumurthy, C.B. (2014) Mouse genome editing using the CRISPR/Cas system. *Curr. Protoc. Hum.Genet*, **83**, 11–27.
11. Quadros, R.M., Miura, H., Harms, D.W., Akatsuka, H., Sato, T., Aida, T., Redder, R., Richardson, G.P., Inagaki, Y., Sakai, D. *et al.* (2017) Easi-CRISPR: a robust method for one-step generation of mice carrying conditional and insertion alleles using long ssDNA donors and CRISPR ribonucleoproteins. *Genome Biol.*, **18**.
12. Miura, H., Quadros, R.M., Gurumurthy, C.B. and Ohtsuka, M. (2018) Easi-CRISPR for creating knock-in and conditional knockout mouse models using long ssDNA donors. *Nat. Protoc.*, **13**, 195–215.
13. Zhu, Y., Beudez, J., Yu, N., Grutter, T. and Zhao, H.B. (2017) P2X2 dominant deafness mutations have no negative effect on wild-type isoform: implications for functional rescue and in deafness mechanism. *Front. Mol. Neurosci.*, **10**, 371.
14. George, B., Swartz, K.J. and Li, M. (2019) Hearing loss mutations alter the functional properties of human P2X2 receptor channels through distinct mechanisms. *Proc. Natl. Acad. Sci. U.S.A*, **116**, 22862–22871.
15. Jarlebark, L.E., Housley, G.D., Raybould, N.P., Vlajkovic, S. and Thorne, P.R. (2002) ATP-gated ion channels assembled from P2X2 receptor subunits in the mouse cochlea. *Neuroreport*, **13**, 1979–1984.

16. Sirko, P., Gale, J.E. and Ashmore, J.F. (2019) Intercellular ca (2+) signalling in the adult mouse cochlea. *J. Physiol.*, **597**, 303–317.
17. Housley, G.D., Kanjhan, R., Raybould, N.P., Greenwood, D., Salih, S.G., Jarlebark, L., Burton, L.D., Setz, V.C., Cannell, M.B., Soeller, C. *et al.* (1999) Expression of the P2X(2) receptor subunit of the ATP-gated ion channel in the cochlea: implications for sound transduction and auditory neurotransmission. *J. Neurosci.*, **19**, 8377–8388.
18. Liu, X.Z., Yan, D., Mittal, R., Ballard, M.E. and Feng, Y. (2019) Progressive dominant hearing loss (autosomal dominant Deafness-41) and P2RX2 gene mutations: a phenotype-genotype study. *Laryngoscope*, in press.
19. Liberman, M.C. (1980) Efferent synapses in the inner hair cell area of the cat cochlea: an electron microscopic study of serial sections. *Hear. Res.*, **3**, 189–204.
20. Liberman, L.D., Wang, H. and Liberman, M.C. (2011) Opposing gradients of ribbon size and AMPA receptor expression underlie sensitivity differences among cochlear-nerve/hair-cell synapses. *J. Neurosci.*, **31**, 801–808.
21. Ruel, J., Wang, J., Rebillard, G., Eybalin, M., Lloyd, R., Pujol, R. and Puel, J.L. (2007) Physiology, pharmacology and plasticity at the inner hair cell synaptic complex. *Hear. Res.*, **227**, 19–27.
22. Fuchs, P.A. and Glowatzki, E. (2015) Synaptic studies inform the functional diversity of cochlear afferents. *Hear. Res.*, **330**, 18–25.
23. Hong, J., Chen, Y., Zhang, Y., Li, J., Ren, L., Yang, L., Shi, L., Li, A., Zhang, T., Li, H. *et al.* (2018) N-methyl-D-aspartate receptors involvement in the gentamicin-induced hearing loss and pathological changes of ribbon synapse in the mouse Cochlear inner hair cells. *Neural Plast.*, **2018**, 3989201.
24. Johnson, S.L., Eckrich, T., Kuhn, S., Zampini, V., Franz, C., Ranatunga, K.M., Roberts, T.P., Masetto, S., Knipper, M., Kros, C.J. *et al.* (2011) Position-dependent patterning of spontaneous action potentials in immature cochlear inner hair cells. *Nat. Neurosci.*, **14**, 711–717.
25. Nouvian, R., Beutner, D., Parsons, T.D. and Moser, T. (2006) Structure and function of the hair cell ribbon synapse. *J. Membr. Biol.*, **209**, 153–165.
26. Yin, Y., Liberman, L.D., Maison, S.F. and Liberman, M.C. (2014) Olivocochlear innervation maintains the normal modiolar-pillar and habenular-cuticular gradients in cochlear synaptic morphology. *J. Assoc. Res. Otolaryngol.*, **15**, 571–583.
27. Liberman, L.D., Suzuki, J. and Liberman, M.C. (2015) Dynamics of cochlear synaptopathy after acoustic overexposure. *J. Assoc. Res. Otolaryngol.*, **16**, 205–219.
28. Liu, K., Chen, D., Guo, W., Yu, N., Wang, X., Ji, F., Hou, Z., Yang, W.Y. and Yang, S. (2015) Spontaneous and partial repair of ribbon synapse in Cochlear inner hair cells after ototoxic withdrawal. *Mol. Neurobiol.*, **52**, 1680–1689.
29. Yuan, X., Liu, H., Li, Y., Li, W., Yu, H. and Shen, X. (2020) Ribbon synapses and hearing impairment in mice after in utero sevoflurane exposure. *Drug. Des. Devel.Ther*, **14**, 2685–2693.
30. Hickman, T.T., Liberman, M.C. and Jacob, M.H. (2015) Adenomatous polyposis coli protein deletion in efferent Olivocochlear neurons perturbs afferent synaptic maturation and reduces the dynamic range of hearing. *J. Neurosci.*, **35**, 9236–9245.
31. Nadar-Ponniah, P.T., Taiber, S., Caspi, M., Koffler-Brill, T., Dror, A.A., Siman-Tov, R., Rubinstein, M., Padmanabhan, K., Luxenburg, C., Lang, R.A. *et al.* (2020) Striatin is required for hearing and affects inner hair cells and ribbon synapses. *Front. Cell. Dev.Biol*, **8**, 615.
32. Maison, S.F., Usubuchi, H. and Liberman, M.C. (2013) Efferent feedback minimizes cochlear neuropathy from moderate noise exposure. *J. Neurosci.*, **33**, 5542–5552.
33. Lu, X., Shu, Y., Tang, M. and Li, H. (2016) Mammalian Cochlear hair cell regeneration and ribbon synapse reformation. *Neural Plast.*, **2016**, 2523458.
34. Liu, K., Jiang, X., Shi, C., Shi, L., Yang, B., Shi, L., Xu, Y., Yang, W. and Yang, S. (2013) Cochlear inner hair cell ribbon synapse is the primary target of ototoxic aminoglycoside stimuli. *Mol. Neurobiol.*, **48**, 647–654.
35. Shi, L., Liu, K., Wang, H., Zhang, Y., Hong, Z., Wang, M., Wang, X., Jiang, X. and Yang, S. (2015) Noise induced reversible changes of cochlear ribbon synapses contribute to temporary hearing loss in mice. *Acta Otolaryngol.*, **135**, 1093–1102.
36. Mittal, R., Grati, M., Sedlacek, M., Yuan, F., Chang, Q., Yan, D., Lin, X., Kachar, B., Farooq, A., Chapagain, P. *et al.* (2016) Characterization of ATPase activity of P2RX2 Cation Channel. *Front. Physiol.*, **7**, 186.